Enzyme like Activity of Cobalt-MOF Nanosheets for Hydrogen Peroxide Electrochemical Sensing

Arismendy Portorreal-Bottier,[a] Silvia Gutiérrez-Tarriño,[b] Juan José Calvente,[a] Rafael Andreu,[a] Emilio Roldán,[a] Pascual Oña-Burgos,[b,c,*] José Luis Olloqui-Sariego[a,*].

[a]*Departamento de Química Física. Universidad de Sevilla. Profesor García González 1. 41012 Sevilla. Spain.*

[b]*Instituto de Tecnología Química, Universitat Politècnica de València-Consejo Superior de Investigaciones Científicas (UPV-CSIC), Avda. de los Naranjos s/n, 46022 Valencia, Spain.*

[c]*Departamento de Química y Física, Centro de Investigación CIAIMBITAL, Universidad de Almería, Ctra. Sacramento, s/n, 04120 Almería, Spain.*

Corresponding Authors

jlolloqui@us.es

pasoabur@upvnet.upv.es

Abstract

Metal-organic frameworks (MOFs) are receiving increased attention as new functional nanomaterials for the development of electrochemical sensors. Herein, we develop an electrochemical platform for non-enzymatic hydrogen peroxide detection built with a composite of two-dimensional cobalt MOF nanosheets and Nafion (2D-Co-MOF@Nafion). The feasibility of the 2D-Co-MOF@Nafion composite as active material for high performance hydrogen peroxide sensor was investigated by using cyclic voltammetry and chronoamperometry. Its voltammetric response reveals an efficient charge transport through the MOF composite, and rapid electron exchange between the MOF and the electrode. Notably, these MOF nanosheets exhibit enzyme-like activity for the non-common catalytic oxidation of hydrogen peroxide, leading to an electrochemical sensor with rapid quantitative detection, outstanding sensitivity, selectivity, stability, and durability at the desirable neutral pH. In particular, for a cobalt metal loading of 1.2 nanomol, the sensor yields amperometric H_2O_2 detection with characteristic electrocatalytic parameters of i_{max} = 5.7 mA cm^{-2} and K_M = 13 mM. Moreover, linear ranges of up to either 1 mM or 10 mM are achieved, with sensitivities as high as 570 ± 5 A cm^{-2} mM^{-1} or 395 ± 10 A cm^{-2} mM^{-1} for the low and high concentration ranges, respectively. The particular coordination chemistry of the MOF consisting of a regular arrangement of multiple Co(II) redox metal sites connected by appropriate organic ligands can provide inherent enzyme-mimicking properties, thereby explaining the higher oxidase-like activity of the present MOF. This work raises the new idea of using two-dimensional cobalt-based MOFs as active nanozymes, offering exciting opportunities in the design of non-enzymatic electrochemical sensing devices.

Keywords: Non-Enzymatic Electrochemical Sensor; 2D Metal-Organic Framework; Electrocatalysis; Oxidase Activity; Hydrogen Peroxide Detection; Neutral pH

1. Introduction

The detection and quantification of H_2O_2 is important in the fields of clinical diagnostics, biotechnology, and industrial manufacture in environmental, food, and industrial analysis, because of its involvement as an oxidizing agent in many chemical, biological, pharmaceutical, and environmental processes. Its concentrations naturally range from micromolar to tens of millimolar.[1] Among other sensing techniques, electrochemical sensors show appealing performance in terms of low cost, fast response, ease of operation, and high sensitivity.[2] Electrochemical detection of H_2O_2 is categorized into two types, namely enzymatic and nonenzymatic. The use of enzymes, and in particular peroxidases, as electrocatalysts has been increasingly studied for the development of enzyme-based electrochemical H_2O_2 sensors, since they offer great benefits in terms of activity and specificity.[1,3,4] However, the use of these enzyme-based electrochemical sensors is strongly limited by their poor stability in non-optimal operating conditions and their inherent suicide inactivation reactions.[1,5,6] Alternatively, nanomaterials with enzyme-like characteristics, called “nanozymes”, are receiving increased attention as appealing non-enzymatic electrochemical platforms for sensing application, since they can overcome the limitations of enzyme-based electrochemical biosensors.[1,7–10] A wide variety of nanostructured materials have proven enzyme-like activity, including carbon, metals and metal oxides.[7,8,11–17] In recent years, many works have been devoted to the synthesis of nanozymes with promising results for biosensing applications. However, the catalytic activity of most nanozymes remain much lower than that of the natural enzymes, so the design and development of highly active nanozyme materials is challenging.[17]

Metal−organic frameworks (MOFs) are a novel class of porous materials that are emerging in the chemical sensing area due to their unique characteristics, such as ultrahigh specific surface area, regular porosity, controllable arrangement of isolated active sites and highly tunable structures, as well as excellent thermal and chemical stability. Besides, in a typical MOF, the enzyme-like catalytic capacity can originate from the added effect of metal redox couples binding to organic ligands that act as electron mediators.[13,18–22] These ligands mimic the

coordination environment of the metal centers in natural enzymes and catalyze the reduction (or oxidation) of substrates in a similar way. However, the research of MOFs as electrochemical sensors is still in an early stage and still constitutes a challenge in the bio- and chemical detection areas. Indeed, traditional MOFs have interconnected 3D structures that suffer from high mass transfer resistance, thereby diminishing the activity of MOF nanozymes.[15] One elegant strategy to solve this limitation is the development of related 2D materials, which provide more exposed electroactive sites, thus improving the electrical conductivity and lowering the diffusion barriers.[15,23–28] So far, few papers have been devoted to the fabrication of electrochemical H_2O_2 sensors based on cobalt MOFs, and most of them use oxy(hydroxide) species derived from the original MOF that operate only in the undesirable strong alkaline medium.[10,29–33] H_2O_2 detection in typical bio- and chemical samples is carried out at circumneutral pHs, at which these cobalt oxide species are expected to decrease their catalytic activity.

Herein, we develop an electrochemical sensor for the detection of H_2O_2 at the desirable, but not commonly employed, neutral pH, consisting of a two-dimensional cobalt MOF (2D-Co-MOF) with a nitrogen coordination environment based on layered double nanosheets, and supported on a graphite electrode. It takes advantage of its previously proven superior catalytic activity for the water electroxidation reaction.[34] Interestingly, we demonstrate that this 2D-Co-MOF exhibits high oxidase-like activity at neutral pH, being able to mediate the catalytic oxidation of H_2O_2, whose novel catalytic properties are ascribed to the particular active metal coordination with several nitrogen-metal bonds. Moreover, this metal coordination in the secondary building unit of the MOF is preserved in the electrode, which is a differential feature with respect to most electrochemical H_2O_2 sensors based on MOFs, since these sensors operate under strongly alkaline conditions where the MOFs undergo a phase transition to form cobalt oxy(hydroxide) species. The so-developed electrode was shown to sense H_2O_2 with high sensitivity and selectivity, fast response time, wide linear range, and high stability, thus revealing enzyme-like

activity. To the best of our knowledge, this electrocatalytic activity of as-synthesized Co-MOF for the electrooxidation of H_2O_2 is unprecedented.

2. Materials and methods

2.1. Synthesis of the Cobalt MOF

Solvothermal conditions were employed to generate Co-MOF, using $[(Co_4O_4)(OAc)_4(py)_4]$[35] as building block, following a reported procedure.[34] Briefly, this MOF was synthesized in autoclave at 150ºC for 9 days under autogenous pressure and static conditions using 4 equivalents of 2,2′-bipyridine-4,4′-dicarboxylic acid (bda) and 8 equivalents of trifluoroacetic acid per each equivalent of $[Co_4O_4(OAc)_4(py)_4]$ which were dissolved in pyridine. Once cooled at room temperature, the solution was filtered, and the collected red crystals were washed with acetone and dried under vacuum at room temperature. Anal. Calculated for $C_{18}H_{11}CoN_3O_4$: C, 55.119; H, 2.827; N, 10.713; Co, 15.025. Found: C, 55.071; H, 3.052; N, 10.773; Co, 15.051.

2.2. Apparatus and measurements

All chemicals were purchased from the Sigma Aldrich Chemical Co. or ABCR and used as received. A CUBIX diffractometer from PANalytical equipped with a PANalytical X'Celerator detector in a Bragg-Bretano geometry was used to acquire the X-ray diffraction measurements according to the powder method. The measurement range was from 2.0º to 40º (2θ) with a step of 0.020º (2θ) and Cu Kα was used as X-ray radiation. Scanning electron microscopy of field emission **(**FESEM) images were acquired using an Ultra 55 (Zeiss), operating at 2.0 kV. A sample holder with double-sided adhesive tape was used for the preparation of the powder samples which were coated with platinum to avoid charging effects. A SPECS spectrometer equipped with a Phoibos 150MCD-9 multichannel analyzer using non monochromatic MgKα (1253.6 eV) irradiation was used for measuring X-ray photoelectron spectra of the catalysts. Spectra were recorded using an analyzer pass energy of 30 eV, an X-ray power of 100W and under an operating pressure of 10^{-9} mbar. Peak intensities were calculated after nonlinear Shirley-type background subtraction and corrected by the transmission function of the

spectrometer. Gaussian-Lorentzian curves were used for peak fitting. C1s peak (284.5 eV) was used for referenced binding energy (BE) values during data processing of the XPS spectra using casa XPS software for the treatment. Raman spectra were recorded on a Renishaw in Raman Spectrometer ("Refelx"), equipped with a CCD detector with a 785 nm laser excitation. The laser power on the sample was between 5 and 50%, and a total of 20 acquisitions were taken for each spectrum.

Electrochemical measurements were performed with an AUTOLAB PGSTAT 30 from Eco Chemie B.V. in a conventional three electrodes undivided glass cell, equipped with a gas inlet, and thermostated with a water jacket. The counter and reference electrodes were a Pt bar and a Ag|AgCl|NaCl sat. electrode, respectively. The rotating disk electrode was operated at 750 rpm. with an AMSFRX analytical rotator from Pine Instruments Co. All measurements were carried out under an argon atmosphere. Working solutions contained 0.1 M sodium phosphate buffer aqueous solution at pH 7. The ohmic drop was compensated using the positive feedback compensation implemented in the instrument.

2.3. Preparation of the Cobalt MOF based Electrochemical Sensor

The working electrode was a homemade pyrolytic graphite electrode constructed by fitting a rod of highly oriented pyrolytic graphite from Mineral Technologies into a PEEK casing, so that it exposed the edge of the graphite planes with a circular geometric area of 0.07 cm^2. Before cobalt MOF coating, graphite electrodes were polished with abrasive P2400 sandpaper, and then rinsed with Millipore water and dried. To modify the electrode, a suspension of 5 mg mL^{-1} of cobalt MOF material in a 1% v/v Nafion solution (5 wt. % in lower aliphatic alcohols and 15-20% water solution, from Sigma Aldrich, diluted with absolute ethanol) was prepared by vigorous stirring with the Vortex for 30 seconds. Then, a ~10 µL of this suspension was drop cast onto the graphite electrode and dried at room temperature overnight. The so-prepared electrode was activated in aqueous sodium phosphate buffer pH 7, by applying a potential of 0.95 V vs. Ag|AgCl|NaCl sat. for 60 minutes.[34]

3. Results and discussion

3. 1. Structural characterization of the Co-MOF@Nafion Composite

The secondary building unit of the cobalt MOF was previously characterized by single crystal X-ray diffraction,[34] revealing that the Co^{2+} atoms lie in a distorted octahedral environment and are six-coordinated by three oxygen atoms from three different bda^{2-} ligands, two nitrogen atoms of one bda^{2-} ligand, different from the three which are coordinated to the cobalt by the carboxylic group, and to a nitrogen atom from a pyridine ligand (Figure 1a). This material extends into two spatial directions, forming a layered material consisting of nanosheets of two single layers with an interplanar distance of 3.491Å (Figure S1), which are further packed into three-dimensional supramolecular structures.

The Co-MOF was crosslinked with Nafion forming a composite material as the building block for the electrochemical sensor. This composite was characterized by Powder X-Ray Diffraction (PXRD), Raman spectroscopy, Field Emission Scanning Electron Microscopy (FESEM), Energy-dispersive X-ray spectroscopy (EDX) and X-ray photoelectron spectroscopy (XPS). The obtained results were compared with the reported ones for the original bare Co-MOF.[25] First, the PXRD spectrum of Co-MOF within the composite (Figure 1b) showed that the π-stacked Co-MOF preserve its structure, but adopts a preferential [100] orientation in the composite, where the crystals of the MOF interact in a planar way with the Nafion. The preservation of the cobalt MOF structure was also confirmed by Raman spectroscopy (Figure 1c), where it can be observed the Raman bands associated with the axially coordinated pyridine ligands (768, 1010, and 1283 cm^{-1}), the bands associated with the bipyridine (774, 1022 and 1278 cm^{-1}) and the ones associated with the carboxylic groups (1289, 1426, 1546 and 1615 cm^{-1}), indicating that the cobalt centers preserve their coordination after the formation of the composite with Nafion.

On the other hand, FESEM images and EDX analysis (Figure 1d) clearly show that cobalt centers are homogeneously distributed in the composite, thus ruling out metal aggregation.

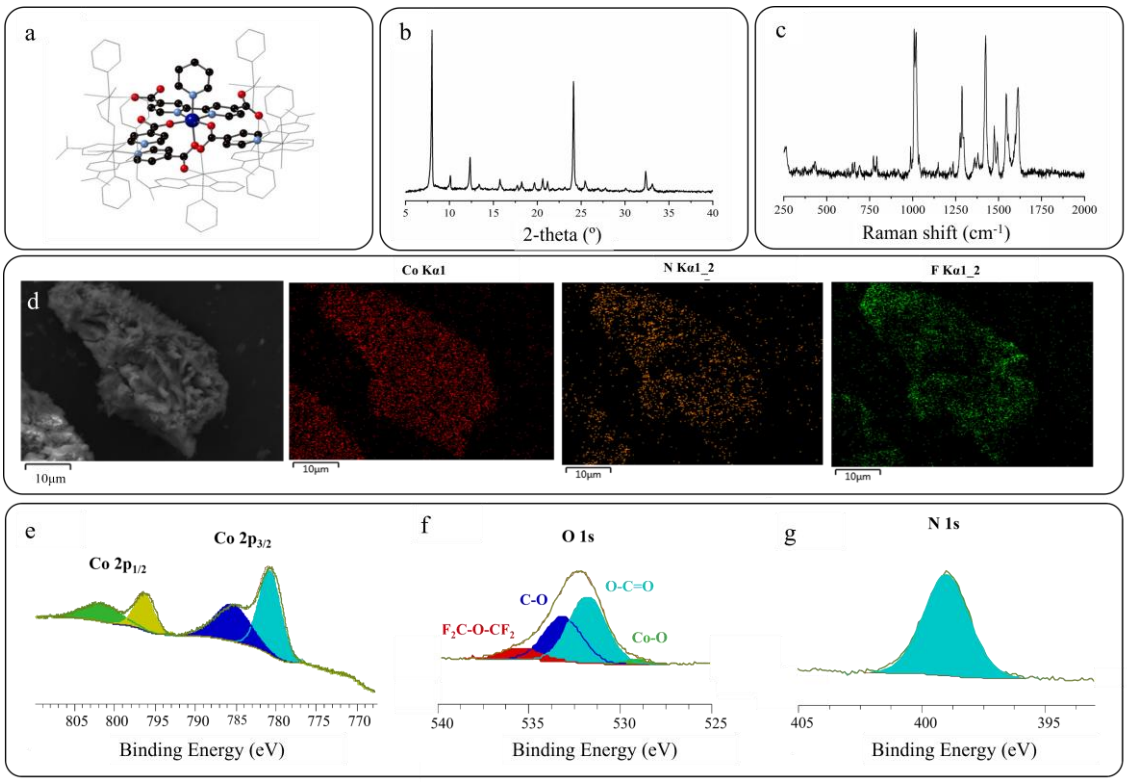

Figure 1. Structural characterization of the Co-MOF@Nafion composite: (a) single-crystal X-ray diffraction structure of the secondary building unit, (b) PXRD spectrum, (c) Raman spectrum, (d) FESEM image and EDX analysis, and XPS spectra of Co 2p line (e), O 1s line (f) and N1s line (g).

Finally, the electronic structure of this material was also analyzed by XPS (Figures 1e-g) to elucidate the nature of the coordination environment. The survey spectrum shows the presence of cobalt, oxygen, carbon, nitrogen, fluorine and sulfur. The analysis of XPS spectra of 2p transition metals is not a straightforward process,[37] for these 3d transition elements. The binding energy (E_b), which is typically used in XPS to determine the oxidation number of a chemical element, is considered as an informative value.[37] According to theoretical calculations,[38] the Co $2p_{1/2}$−Co $2p_{3/2}$ spin−orbit splitting increases when the number of the unpaired 3d electrons is increased, being closer to 16 eV for high-spin Co(II) and to 15 eV for

Co(III). For the current Co-MOF@Nafion composite, E_b(Co $2p_{3/2}$), E_b(Co $2p_{1/2}$) and ΔE_1 values are 780.7, 796.4 and 15.7 eV, respectively (Figure 1f). Furthermore, intense satellite peaks ($\Sigma sat/ICo_{2p} > 1.6$) have been observed for the Co $2p_{3/2}$ spectra. Both $\Sigma sat/ICo_{2p}$ and ΔE_1 values are characteristic of the high spin cobalt(II) compounds,[39–42] indicating that the cobalt centers maintain the same Co(II) oxidation state in the composite.

Interestingly, as evidenced by comparing the Raman spectra of the pristine Co-MOF before and after water treatment (Figure S2),[34] Co-MOF in the composite instantaneously delaminates in contact with an aqueous solution, triggered by the replacement of the axial pyridine ligands by water molecules, producing individual double nanosheets of the MOF (2D-Co-MOF). This depillarization process, involving the mentioned pyridine-water ligand exchange, opens metal sites in the MOF that are adequate for carrying catalytic reactions and, more importantly, the 2D-Co-MOF maintains its structural features.

3. 2. Electrochemical Performance of 2D-Co-MOF@Nafion/PG electrodes for H_2O_2 Detection

Voltammetric Response. First, the electrocatalytic activity of the 2D-Co-MOF@Nafion nanocomposite was evaluated by cyclic voltammetry in a 0.1 M sodium phosphate buffer (SPB) solution at pH 7 and 25 ºC (Figure 2). In the absence of hydrogen peroxide (black line in Figure 2), the voltametric response of the 2D-Co-MOF@Nafion-modified electrode consists of a quasi-reversible voltammetric wave with a midpoint potential of 0.80 ± 0.01 V (vs. Ag|AgCl|NaCl sat.), that can be attributed to the Co(II)/Co(III) redox conversion. Besides, the midpoint potential becomes systematically more positive (by ~100 mV) upon increasing the scan rate, reflecting differences in the MOF environment across the film (Figures S3 in SI). Information on electron transfer kinetics can be obtained from the dependence of the voltammetric peak potential separation (*ΔEp*) on the potential scan rate (see Figures S3 in SI). The independence of *ΔEp* on the scan rate at low scan rates agrees with the expected behavior for a fast charge transport across a multilayer.[43,44] However, at high scan rates, the redox conversion approaches the linear *ΔEp* vs. ln *v* behavior expected for a kinetically controlled

electron transfer of a homogeneous redox thin layer, which can be attributed to the electron exchange of the adjacent catalyst close to the electrode surface. A value of the apparent heterogeneous electron transfer rate constant k_s^{app} of 7.5 s^{-1} was determined from the Butler-Volmer formalism.

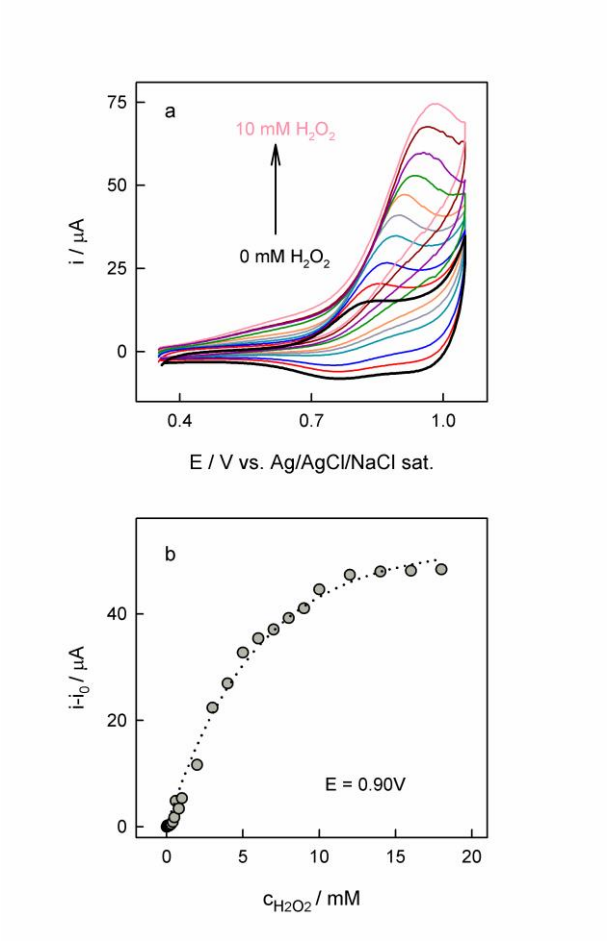

Figure 2. (a) Cyclic voltammograms recorded at 0.01 V s^{-1} after successive additions of hydrogen peroxide to the cell solution and (b) its corresponding calibration plot at 0.90 V of a pyrolytic graphite electrode coated with 2D-Co-MOF@Nafion composite. Other experimental conditions, 0.1 M SPB pH 7.0 and 25 ºC.

Furthermore, integration of the area under the anodic voltammetric peak recorded at low potential scan rates provides the amount of electroactive cobalt centers (~ 1.1 ± 0.3·10^{-9} mol), whose magnitude indicates that a large population of cobalt centers is in effective electrical contact with the electrode and, likewise, reveals an effective charge transport across the

composite. Indeed, it has previously been proven that the laminar morphology of the MOF in the composite provides outstanding ionic migration and electron transfer across the film.[34] Additionally, the obtained electrochemical impedance spectra (Figure S4) measured at 0.92 V with an AC perturbation of 5 mV in the frequency range between 100 kHz and 0.1 Hz for the modified electrode is consistent with the expected responses for the redox conversion of a 3D film controlled by the electron diffusion across the film, under conditions where both the ionic migration and the electron exchange between the electrode and the nearby redox centers are fast.

Notably, upon addition of hydrogen peroxide, the 2D-Co-MOF@Nafion-based electrode produces well developed peak-shaped electrocatalytic waves (Figure 2), characteristic of substrate diffusion control, thereby consistent with a highly efficient electron transport across the MOF film. Redox mediation of the catalytic H_2O_2 oxidation by the 2D-Co-MOF has been further corroborated by comparing the voltammetric responses of the 2D-Co-MOF@Nafion electrode and the solely Nafion-based electrode in the presence of hydrogen peroxide (Figure S5).

The corresponding calibration plot, obtained from the voltammetric currents at 0.90 V after successive additions of hydrogen peroxide to the cell solution, closely matches the typical saturation curve for a Michaelis–Menten reaction scheme. This is characterized by an initial linear dependence of the catalytic current with the hydrogen peroxide concentration and tends to a limiting value for a sufficiently high substrate concentration. Interestingly, the sensor exhibits a very wide linear range, which is consistent with a large number of catalytic metal centers in the composite. Moreover, these results reveal an efficient electrocatalytic activity of the 2D-Co-MOF to mediate the hydrogen peroxide oxidation through the redox conversion of the metal nodes. To the best of our knowledge, this catalytic “oxidase” activity of a cobalt-based MOF is unprecedented, and can be explained by the particular coordination chemistry of the MOF consisting of a regular arrangement of multiple Co(II) redox metal sites connected by appropriate organic ligands, which mimics to some extent the redox cofactor environment of the

enzymes. In addition, the electrochemical stability of the sensor has been assessed by recording five consecutives cyclic voltammograms in the absence or in the presence of 1mM hydrogen peroxide (Figure S6). It can be observed that, in both cases, the voltammetric response remains unchanged, thus proving a good scanning stability of the modified electrode.

Amperometric Response. To investigate the feasibility of the 2D-Co-MOF@Nafion-based electrode as practical hydrogen peroxide amperometric sensors, chronoamperometric measurements were performed at an applied potential of 0.9 V. The current response was recorded during successive additions of hydrogen peroxide to the cell solution every 100 s at a rotation speed of 750 rpm. A typical chronoamperogram is depicted in Figure 3a. It reveals that the current quickly reaches a steady state value after each addition, and it increases with the hydrogen peroxide concentration in a wide range.

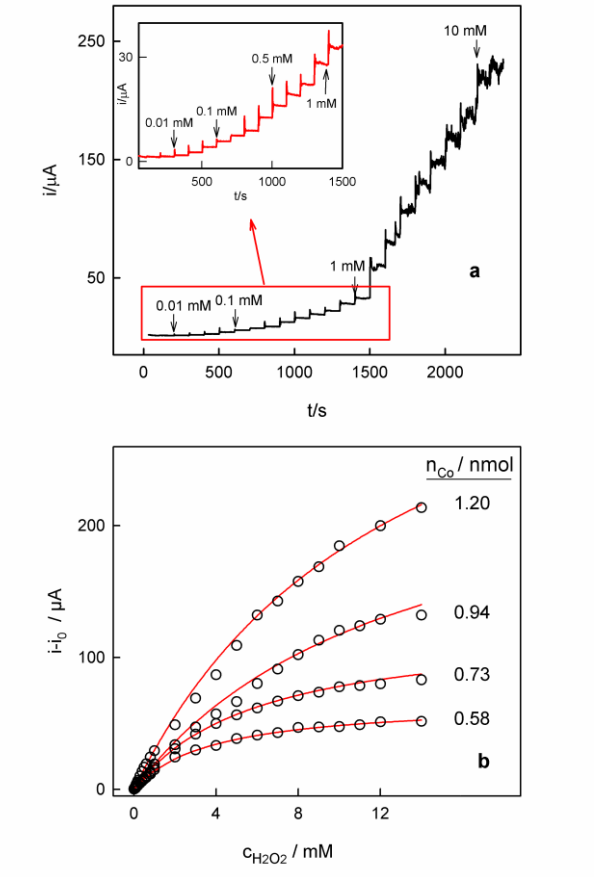

Figure 3. (a) Chronoamperometric curve recorded at 0.90 V and 750 rpm after successive additions of hydrogen peroxide to the cell solution, within the hydrogen peroxide concentration range of 0-12 mM, of a pyrolytic graphite electrode coated with 2D-Co-MOF@Nafion composite with $1.20 \cdot 10^{-9}$ mol of electroactive cobalt centers. (b) The dependence of the electrocatalytic current on hydrogen peroxide concentration of a pyrolytic graphite electrode coated with 2D-Co-MOF@Nafion composite with different amount of electroactive cobalt centers. Open symbols are experimental values, and lines are theoretical fits computed from eq. 1 with the parameter values collected in the SI. Other experimental conditions, 0.1 M SPB pH 7.0 and 25 ºC.

Moreover, chronoamperometric experiments varying the MOF surface coverage on the electrode were performed, and their calibration plots are illustrated in Figure 3b. It turns out that both the linear response range and the limiting current increase with the amount of electroactive cobalt centers in the MOF, reflecting that the cobalt loading has a strong effect on the sensing operational parameters of the electrochemical sensor. We have found that this behavior can be reproduced by using the Michaelis-Menten equation:

$$i_{cat} = \frac{i_{max}\ \mathrm{c}_{H_2O_2}}{K_M + \mathrm{c}_{H_2O_2}} \qquad (1)$$

where K_M is the Michaelis constant and i_{max} is the maximum electrocatalytic current for the hydrogen peroxide oxidation. Satisfactory fits were obtained by using the characteristic parameters derived from the double-reciprocal plots of the normalized catalytic current vs. hydrogen peroxide concentration for each cobalt loading (Figure S7). The intercepts and slopes provide the i_{max} and K_M/i_{max} values (Table S1), respectively.

Moreover, the dependence of the electrocatalytic current, normalized by the amount of electroactive cobalt centers, on the hydrogen peroxide concentration is shown in Figure 4. The corresponding calibration curve (steady-state catalytic current vs. H_2O_2 concentration) is characterized by an excellent linearity in the wide range of 5 μM-10 mM with a coefficient determination of $r^2 = 0.997$. The sensitivity of the sensor estimated from the slope of the calibration curve was 0.501 ± 0.003 A cm^{-2} mM^{-1} μmol^{-1} of electroactive cobalt centers. For an improved sensitivity, the calibration curve can be fitted in two similar linear regions (amplified in Figure 4). Thus, in the hydrogen peroxide concentration range from 5 μM to 1 mM, the

obtained linear regression equation was y = 0.684 x + 0.00984 (with r^2 = 0.996), whereas in the hydrogen peroxide concentration range of 1 mM to 10 mM the linear regression equation was y = 0.474 x + 0.290 (with r^2 = 0.998). It should be noted that the small error associated with the estimation of the sensitivity normalized to the amount of electroactive cobalt for eight different electrodes, clearly reflects a very good reproducibility of the current MOF-based electrochemical sensor.

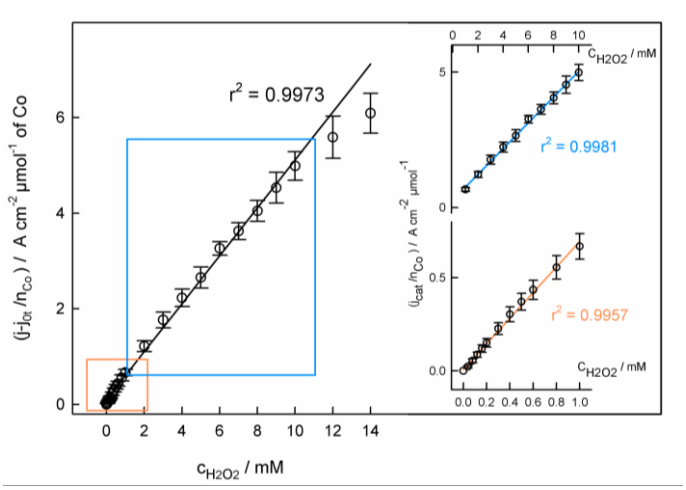

Figure 4. (a) The dependence of the electrocatalytic current normalized by the amount of electroactive cobalt centers on hydrogen peroxide concentration of a pyrolytic graphite electrode coated with 2D-Co-MOF@Nafion composite. Inset plots shows a close look with the hydrogen peroxide concentration from 0 mM to 1 mM (bottom) and from 1 mM to 10 mM (top). Solid lines are the best linear least-square fits to the data. Other experimental conditions: 0.1 M SPB, pH 7.0, 25 ºC and electrode rotation rate 750 rpm.

In addition, given that the maximum surface coverage of electroactive cobalt centers reached in this work was 1.2 nmol, the corresponding sensitivities were as high as 570 ± 5 A cm^{-2} mM^{-1} and 395 ± 10 A cm^{-2} mM^{-1} for the low and high concentration ranges, respectively. Comparison of the operating parameters of the so-fabricated hydrogen peroxide sensor with those previously reported for electrochemical sensors based on genuine or derived cobalt MOF materials reveals superior sensing performance (see Table S3).

The selectivity of this sensor was assessed by measuring the influence of some easily oxidizable compounds present in the physiological and environmental samples on the electrocatalytic current of H_2O_2. In particular, we monitored the steady state electrocatalytic current after successive addition of 0.5 mM glucose, ascorbic acid (AA), oxalic acid (OA) and uric acid (UA) to a solution containing 1 mM H_2O_2 (Figure 5a). As can be observed the current remained unchanged after addition of all these species, revealing a good selectivity of the MOF even in the presence of common interferences, likely induced by the selective interaction between the substrate and the cobalt center. The latter is consistent with a Co-H_2O_2 binding equilibrium as an intermediate step in the catalytic mechanism.

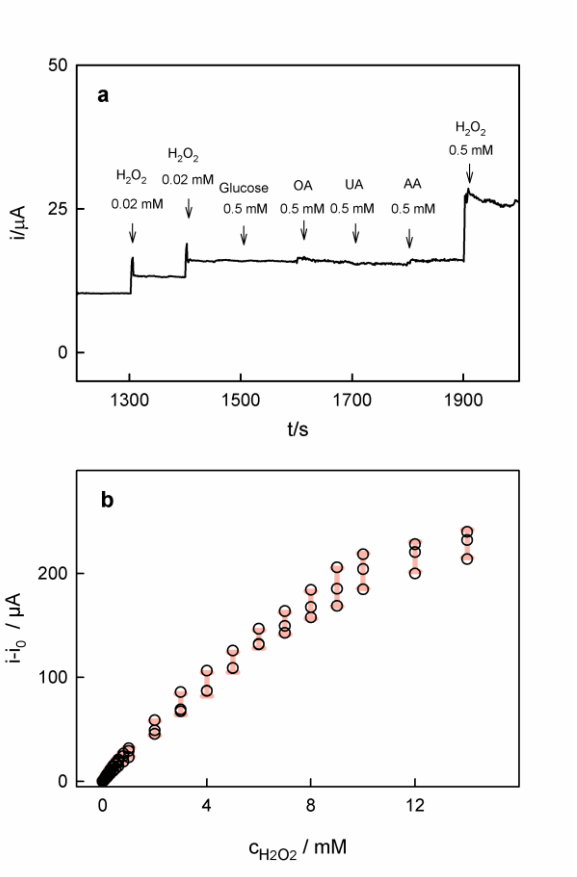

Figure 5. (a) Chronoamperometric curve recorded at 0.90 V for a pyrolytic graphite electrode coated with 2D-Co-MOF@Nafion composite after the indicated additions of hydrogen peroxide, glucose, oxalic acid (OA), uric acid (UA) and ascorbic acid (AA) to the cell solution. (b) Calibrations curves for three successive chronoamperometric experiments using the same 2D-Co-MOF@Nafion-modified electrode. Other experimental conditions: 0.1 M SPB, pH 7.0, 25 ºC and electrode rotation rate 750 rpm.

The repeatability of the sensor was also assessed by measuring three successive calibration curves for H_2O_2 with the same electrode (Figure 5b). Their similarity reveals a good reusability of the sensor (Figure 5b).

Furthermore, the effect of the applied potential on the Co-MOF-mediated hydrogen peroxide electrocatalytic oxidation was also assessed to elucidate the rate determinant step of the overall electrocatalytic reaction. Figures 6a and 6b depict the chronoamperograms recorded as a function of both the applied potential and substrate concentration and their corresponding calibration plots at pH 7.0, respectively. It can be seen that the catalytic current increases with both the applied potential and the hydrogen peroxide concentration until it reaches a saturation limit at sufficiently positive potentials. Accordingly, the corresponding calibration plots (electrocatalytic current normalized by the electrode surface area and the amount of cobalt active sites versus hydrogen peroxide concentration) at different applied potentials show a biphasic behavior, which can be reproduced quantitatively with eq 1 and the i_{max} and K_M values determined from the corresponding double-reciprocal plots (Figure S8 and Table S2). In the relatively low hydrogen peroxide concentration range (< 1 mM), the catalytic oxidation rate depends linearly on the hydrogen peroxide concentration but is nearly potential insensitive. This behavior is consistent with an overall catalytic reaction limited by the chemical step involving the substrate, likely the formation of the Michaelis-Menten intermediate complex. In the relatively high hydrogen peroxide concentration range (> 1 mM), the catalytic current tends to the saturation limit, which strongly depends on the applied potential. This behavior agrees with a preceding electrochemical limiting step, where the overall electrocatalytic current is determined by the number of active Co(III) centers, which in turn are modulated by the applied potential (reaction 1). For applied potentials higher than 0.98 V, the calibration plots are virtually the same, indicating that the electrocatalytic rate for hydrogen peroxide oxidation is limited by the proper catalytic reaction (reactions 2-7).

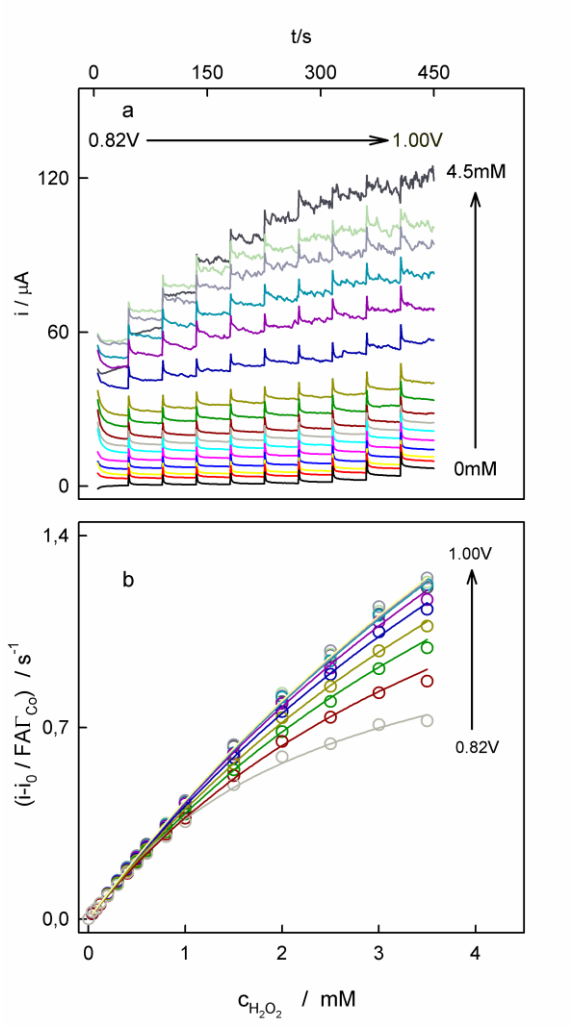

Figure 6. (a) Chronoamperometric curve recorded within the potential range of 0.82 - 1.00 V and potential within the hydrogen peroxide concentrations range of 0.08 – 4.5 mM. (b) Their corresponding calibration plots of the normalized electrocatalytic currents as a function of the hydrogen peroxide concentration as a function of applied potential. Open symbols are experimental values, and lines are theoretical fits computed from eq. 1 with the parameter values collected in the SI. Other experimental conditions: 0.1 M SPB, pH 7.0, 25 ºC and electrode rotation rate 750 rpm.

Based on these results, two plausible mechanisms for the electrocatalytic oxidation of hydrogen peroxide mediated by the electrogenerated Co(III) is proposed. The first step involves the electrochemical oxidation of Co(II) MOF to form the catalytically active Co(III) redox state (reaction 1).

$$Co^{2+} \longrightarrow Co^{3+} + e^{-}\ (electrode) \quad (1)$$

From a mechanistic point of view, the saturation of the electrocatalytic current at sufficiently high H_2O_2 concentrations suggests the formation of an adduct between the electrogenerated Co(III) centers and the hydrogen peroxide molecule (reaction 2):

$$Co^{3+} + H_2O_2 \rightleftarrows Co^{3+} \cdot O_2H_2 \quad (2)$$

Then, oxidation of the bound H_2O_2 would involve a subsequent heterogeneous electron transfer (reaction 3):

$$Co^{3+} \cdot O_2H_2 \longrightarrow Co^{2+} + O_2 + 2H^{+} + e^{-}(electrode) \quad (3)$$

or the alternative homogeneous pathway assisted by the generation of reactive oxygen species (reaction 5-8) [45]:

$$Co^{3+} \cdot O_2H_2 \longrightarrow Co^{2+} + O_2^{\bullet -} + 2H^{+} \quad (4)$$

$$Co^{3+} \cdot O_2H_2 \longrightarrow Co^{2+} + HO_2^{\bullet} + H^{+} \quad (5)$$

$$HO_2^{\bullet} \longrightarrow O_2^{\bullet -} + H^{+} \quad (6)$$

$$Co^{3+} + O_2^{\bullet -} \longrightarrow Co^{2+} + O_2 \quad (7)$$

$$Co^{3+} \cdot O_2H_2 + O_2^{\bullet -} \longrightarrow Co^{2+} + O_2 + H_2O_2 \quad (8)$$

It should be noted that evidence for the formation of a $Co^{3+}\cdot O_2H_2$ adduct has recently been reported by Lehene et al for the nitrogen-coordinated cobalt-containing cobalamin.[46] Furthermore, Nichols et al. have proposed an intermediate Co(III)-hydroperoxide species in the electrocatalytic oxygen reduction mediated by a bipyridine-based Co(III)(N_2O_2) complex.[47]

The structural stability of the 2D-CoMOF in the presence of hydrogen peroxide was further assessed by ex-situ structural characterization of the cobalt MOF composite after exhaustive electrooxidation of hydrogen peroxide in an aqueous solution containing 5 mM of hydrogen peroxide. The corresponding PXRD, Raman and XPS spectra (Figure S9) reveal that the 2D-Co-MOF@Nafion composite maintains its structure, the coordination sphere, and electronic structure, reflecting the high robustness of the as-synthesized MOF.

Finally, the practical applicability of 2D-Co-MOF@Nafion based electrode was tested with commercial lens cleaning solutions spiked with 0.1M H_2O_2, and with a commercial disinfectant sample (6% wt and diluted with buffer to a final concentration of 0.1M H_2O_2). The

amperometric i–t response was recorded by injecting the standard and real samples in the solution cell, each addition corresponding to an increase of the H_2O_2 concentration of 500 μM (Figure S10). The practical analytical parameters are collected in Table S4. It was found that the sensor exhibits average recoveries of 97% and 103%, and RDS of 3.2% and 6.1% for the disinfectant and lens solutions, respectively, reflecting the potential applicability and high accuracy of this MOF-based electrode for the detection of H_2O_2.

Conclusions

In summary, a novel electrochemical platform based on cobalt MOF nanosheets deposited onto a graphite electrode has been developed for hydrogen peroxide sensing. This electrochemical sensor operates through the electrocatalytic oxidation of H_2O_2 mediated by the cobalt centers of the MOF. The dependence of the electrocatalytic current on the hydrogen peroxide concentration follows a Michaelis-Menten pattern, which reveals an unprecedented catalytic "oxidase" activity of the current MOF. This can be tentatively ascribed to the particular coordination chemistry of the cobalt centers in the MOF, where they are linked to oxygen- and nitrogen-containing organic ligands, similar to those found in the enzyme prosthetic groups. The fast electron transport across the film is exploited to improve the electrocatalytic activity of the sensor by increasing the population of cobalt centers. An in-depth structural characterization of the Co-MOF, before and after extensive hydrogen peroxide electrooxidation, reveals its high structural stability. Thus, this material satisfies two requirements for its use as a building block in H_2O_2 sensing, namely an efficient and stable electrocatalytic activity.

Overall, this work shows that Co-MOF nanosheets are a promising material for application in electroanalysis, because of the large number of cobalt centers arranged periodically in the space that undergo fast redox conversion with good accessibility to the electrolyte solvent.

Acknowledgments

Authors thank the financial support by the Spanish Government (RTI2018-096399-A-I00) and Junta de Andalucía (P20_01027 and PYC 20 RE 060 UAL).

References

[1] K. Dhara, D.R. Mahapatra, Recent advances in electrochemical nonenzymatic hydrogen peroxide sensors based on nanomaterials: a review, J. Mater. Sci. 54 (2019) 12319–12357. https://doi.org/10.1007/s10853-019-03750-y.

[2] M.H.S. Benjamin J. Privett, Jae Ho Shin, Electrochemical sensors, Anal. Chem. 80 (2008) 4499–4517. https://doi.org/10.1016/B978-0-12-813886-1.00004-8.

[3] P. Bollella, L. Gorton, Enzyme based amperometric biosensors, Curr. Opin. Electrochem. 10 (2018) 157–173. https://doi.org/10.1016/j.coelec.2018.06.003.

[4] J.L. Olloqui-Sariego, J.J. Calvente, R. Andreu, Immobilizing redox enzymes at mesoporous and nanostructured electrodes, Curr. Opin. Electrochem. 26 (2021) 100658. https://doi.org/10.1016/j.coelec.2020.100658.

[5] J.L. Olloqui-Sariego, G.S. Zakharova, A.A. Poloznikov, J.J. Calvente, D.M. Hushpulian, L. Gorton, R. Andreu, Fenton-like inactivation of tobacco peroxidase electrocatalysis at negative potentials, ACS Catal. 6 (2016) 7452–7457. https://doi.org/10.1021/acscatal.6b01839.

[6] J.L. Olloqui-Sariego, G.S. Zakharova, A.A. Poloznikov, J.J. Calvente, D.M. Hushpulian, L. Gorton, R. Andreu, Interprotein Coupling Enhances the Electrocatalytic Efficiency of Tobacco Peroxidase Immobilized at a Graphite Electrode, Anal. Chem. 87 (2015) 10807–10814. https://doi.org/10.1021/acs.analchem.5b01710.

[7] S. Campuzano, M. Pedrero, P. Yáñez-Sedeño, J.M. Pingarrón, Nanozymes in electrochemical affinity biosensing, Microchim. Acta. 187 (2020) 423. https://doi.org/10.1007/s00604-020-04390-9.

[8] P.V.V. Romanholo, C.A. Razzino, P.A. Raymundo-Pereira, T.M. Prado, S.A.S. Machado, L.F. Sgobbi, Biomimetic electrochemical sensors: New horizons and challenges in biosensing applications, Biosens. Bioelectron. 185 (2021) 113242.

https://doi.org/10.1016/j.bios.2021.113242.

[9] X. Xiong, C. You, X. Cao, L. Pang, R. Kong, X. Sun, Ni2P nanosheets array as a novel electrochemical catalyst electrode for non-enzymatic H2O2 sensing, Electrochim. Acta. 253 (2017) 517–521. https://doi.org/10.1016/j.electacta.2017.09.104.

[10] Z. Wu, L.P. Sun, Z. Zhou, Q. Li, L.H. Huo, H. Zhao, Efficient nonenzymatic H2O2 biosensor based on ZIF-67 MOF derived Co nanoparticles embedded N-doped mesoporous carbon composites, Sensors Actuators, B Chem. 276 (2018) 142–149. https://doi.org/10.1016/j.snb.2018.08.100.

[11] Q. Chen, C. Ma, S. Yan, J. Liang, K. Dong, Y. Luo, Q. Liu, T. Li, Y. Wang, L. Yue, B. Zheng, Y. Liu, S. Gao, Z. Jiang, W. Li, X. Sun, Greatly Facilitated Two-Electron Electroreduction of Oxygen into Hydrogen Peroxide over TiO2by Mn Doping, ACS Appl. Mater. Interfaces. 13 (2021) 46659–46664. https://doi.org/10.1021/acsami.1c13307.

[12] A. Payal, S. Krishnamoorthy, A. Elumalai, J.A. Moses, C. Anandharamakrishnan, A Review on Recent Developments and Applications of Nanozymes in Food Safety and Quality Analysis, Food Anal. Methods. 14 (2021) 1537–1558. https://doi.org/10.1007/s12161-021-01983-9.

[13] L. Zhang, J. Liang, L. Yue, K. Dong, Z. Xu, T. Li, Q. Liu, Y. Luo, Y. Liu, S. Gao, A.M. Asiri, Q. Kong, X. Guo, X. Sun, CoTe nanoparticle-embedded N-doped hollow carbon polyhedron: an efficient catalyst for H2O2electrosynthesis in acidic media, J. Mater. Chem. A. 9 (2021) 21703–21707. https://doi.org/10.1039/d1ta06313h.

[14] Z. Xu, J. Liang, Y. Wang, K. Dong, X. Shi, Q. Liu, Y. Luo, T. Li, Y. Jia, A.M. Asiri, Z. Feng, Y. Wang, D. Ma, X. Sun, Enhanced Electrochemical H2O2Production via Two-Electron Oxygen Reduction Enabled by Surface-Derived Amorphous Oxygen-Deficient TiO2- x, ACS Appl. Mater. Interfaces. 13 (2021) 33182–33187. https://doi.org/10.1021/acsami.1c09871.

[15] X. Niu, X. Li, Z. Lyu, J. Pan, S. Ding, X. Ruan, W. Zhu, D. Du, Y. Lin, Metal-organic framework based nanozymes: promising materials for biochemical analysis, Chem. Commun. 56 (2020) 11338–11353. https://doi.org/10.1039/d0cc04890a.

[16] D. Jiang, D. Ni, Z.T. Rosenkrans, P. Huang, X. Yan, W. Cai, Nanozyme: New horizons for responsive biomedical applications, Chem. Soc. Rev. 48 (2019) 3683–3704. https://doi.org/10.1039/c8cs00718g.

[17] Y. Huang, J. Ren, X. Qu, Nanozymes: Classification, Catalytic Mechanisms, Activity Regulation, and Applications, Chem. Rev. 119 (2019) 4357–4412. https://doi.org/10.1021/acs.chemrev.8b00672.

[18] S. Li, X. Liu, H. Chai, Y. Huang, Recent advances in the construction and analytical applications of metal-organic frameworks-based nanozymes, TrAC - Trends Anal. Chem. 105 (2018) 391–403. https://doi.org/10.1016/j.trac.2018.06.001.

[19] X. Niu, X. Li, Z. Lyu, J. Pan, S. Ding, X. Ruan, W. Zhu, D. Du, Y. Lin, Metal-organic framework based nanozymes: promising materials for biochemical analysis, Chem. Commun. 56 (2020) 11338–11353. https://doi.org/10.1039/d0cc04890a.

[20] Y. Wang, Y. Zhu, A. Binyam, M. Liu, Y. Wu, F. Li, Discovering the enzyme mimetic activity of metal-organic framework (MOF) for label-free and colorimetric sensing of biomolecules, Biosens. Bioelectron. 86 (2016) 432–438. https://doi.org/10.1016/j.bios.2016.06.036.

[21] Y. Qiu, G. Tan, Y. Fang, S. Liu, Y. Zhou, A. Kumar, M. Trivedi, D. Liu, J. Liu, Biomedical applications of metal-organic framework (MOF)-based nano-enzymes, New J. Chem. 45 (2021) 20987–21000. https://doi.org/10.1039/d1nj04045f.

[22] S. Rojas-Buzo, P. Concepción, J.L. Olloqui-Sariego, M. Moliner, A. Corma, Metalloenzyme-Inspired Ce-MOF Catalyst for Oxidative Halogenation Reactions, ACS Appl. Mater. Interfaces. 13 (2021) 31021–31030. https://doi.org/10.1021/acsami.1c07496.

[23] C. Xu, L. Liu, C. Wu, K. Wu, Unique 3D heterostructures assembled by quasi-2D Ni-MOF and CNTs for ultrasensitive electrochemical sensing of bisphenol A, Sensors Actuators, B Chem. 310 (2020) 127885. https://doi.org/10.1016/j.snb.2020.127885.

[24] X. Xiao, L. Zou, H. Pang, Q. Xu, Synthesis of micro/nanoscaled metal-organic frameworks and their direct electrochemical applications, Chem. Soc. Rev. 49 (2020) 301–331. https://doi.org/10.1039/c7cs00614d.

[25] H. Li, J. Hou, T.D. Bennett, J. Liu, Y. Zhang, Templated growth of vertically aligned 2D metal-organic framework nanosheets, J. Mater. Chem. A. 7 (2019) 5811–5818. https://doi.org/10.1039/c8ta07234e.

[26] A. Dhakshinamoorthy, A.M. Asiri, H. Garcia, 2D Metal–Organic Frameworks as Multifunctional Materials in Heterogeneous Catalysis and Electro/Photocatalysis, Adv. Mater. 31 (2019) 1900617. https://doi.org/10.1002/adma.201900617.

[27] M. Zhao, Y. Huang, Y. Peng, Z. Huang, Q. Ma, H. Zhang, Two-dimensional metal-organic framework nanosheets: Synthesis and applications, Chem. Soc. Rev. 47 (2018) 6267–6295. https://doi.org/10.1039/c8cs00268a.

[28] S. Yang, N. Xia, M. Li, P. Liu, Y. Wang, L. Qu, Facile synthesis of a zeolitic imidazolate framework-8 with reduced graphene oxide hybrid material as an efficient electrocatalyst for nonenzymatic H2O2 sensing, RSC Adv. 9 (2019) 15217–15223. https://doi.org/10.1039/c9ra02096a.

[29] L. Yang, C. Xu, W. Ye, W. Liu, An electrochemical sensor for H2O2 based on a new Co-metal-organic framework modified electrode, Sensors Actuators, B Chem. 215 (2015) 489–496. https://doi.org/10.1016/j.snb.2015.03.104.

[30] Q.Q. Xiao, D. Liu, Y.L. Wei, G.H. Cui, A new multifunctional two-dimensional cobalt(II) metal–organic framework for electrochemical detection of hydrogen peroxide, luminescent sensing of metal ions, and photocatalysis, Polyhedron. 158 (2019) 342–351. https://doi.org/10.1016/j.poly.2018.11.016.

[31] Y.S. Chang, J.H. Li, Y.C. Chen, W.H. Ho, Y. Da Song, C.W. Kung, Electrodeposition of pore-confined cobalt in metal–organic framework thin films toward electrochemical H2O2 detection, Electrochim. Acta. 347 (2020) 136276. https://doi.org/10.1016/j.electacta.2020.136276.

[32] D. Zhang, J. Zhang, H. Shi, X. Guo, Y. Guo, R. Zhang, B. Yuan, Redox-active microsized metal-organic framework for efficient nonenzymatic H2O2 sensing, Sensors Actuators, B Chem. 221 (2015) 224–229. https://doi.org/10.1016/j.snb.2015.06.079.

[33] B. Liu, X. Wang, Y. Zhai, Z. Zhang, H. Liu, L. Li, H. Wen, Facile preparation of well conductive 2D MOF for nonenzymatic detection of hydrogen peroxide: Relationship between electrocatalysis and metal center, J. Electroanal. Chem. 858 (2020) 113804. https://doi.org/10.1016/j.jelechem.2019.113804.

[34] S. Gutiérrez-Tarriño, J.L. Olloqui-Sariego, J.J. Calvente, G.M. Espallargas, F. Rey, A. Corma, P. Oña-Burgos, Cobalt Metal-Organic Framework Based on Layered Double Nanosheets for Enhanced Electrocatalytic Water Oxidation in Neutral Media, J. Am. Chem. Soc. 142 (2020) 19198–19208. https://doi.org/10.1021/jacs.0c08882.

[35] A.I. Nguyen, M.S. Ziegler, P. Oña-Burgos, M. Sturzbecher-Hohne, W. Kim, D.E. Bellone, T.D. Tilley, Mechanistic Investigations of Water Oxidation by a Molecular Cobalt Oxide Analogue: Evidence for a Highly Oxidized Intermediate and Exclusive Terminal Oxo Participation, J. Am. Chem. Soc. 137 (2015) 12865–12872. https://doi.org/10.1021/jacs.5b08396.

[36] S. Gutiérrez-Tarriño, J.L. Olloqui-Sariego, J.J. Calvente, G.M. Espallargas, F. Rey, A. Corma, P. Oña-Burgos, Cobalt metal-organic framework based on layered double nanosheets for enhanced electrocatalytic water oxidation in neutral media, J. Am. Chem. Soc. 142 (2020) 19198–19208. https://doi.org/10.1021/jacs.0c08882.

[37] M.C. Biesinger, B.P. Payne, A.P. Grosvenor, L.W.M. Lau, A.R. Gerson, R.S.C. Smart, Resolving Surface Chemical States in XPS Analysis of First Row Transition Metals,

Oxides and Hydroxides: Cr, Mn, Fe, Co and Ni, Appl. Surf. Sci. 257 (2011) 2717–2730. https://doi.org/10.1016/j.apsusc.2010.10.051.

[38] T. Ivanova, A. Naumkin, A. Sidorov, I. Eremenko, M. Kiskin, X-Ray Photoelectron Spectra and Electron Structure of Polynuclear Cobalt Complexes, J. Electron Spectros. Relat. Phenomena. 156–158 (2007) 200–203. https://doi.org/10.1016/j.elspec.2006.12.005.

[39] Y. Okamoto, H. Nakano, T. Imanaka, S. Teranishi, X-Ray Photoelectron Spectroscopic Studies of Catalysts — Supported Cobalt Catalysts —, Bull. Chem. Soc. Jpn. 48 (1975) 1163–1168. https://doi.org/10.1246/bcsj.48.1163.

[40] D. Briggs, V.A. Gibson, Direct Observation Of Multiplet Splitting In 2p Photoelectron Peaks Of Cobalt Complexes., Chem. Phys. Lett. 25 (1974) 493–496.

[41] J.C. Carver, G.K. Schweitzer, T.A. Carlson, Use of X- Ray Photoelectron Spectroscopy to Study Bonding in Cr, Mn, Fe, and Co Compounds, J. Chem. Phys. 57 (1972) 973–982. https://doi.org/10.1063/1.1678348.

[42] I.S. D. C. Frost, C. A. McDowell, Woolsey, X-ray Photoelectron Spectra of Cobalt Compounds, Moleular Phys. 27 (1974) 1473–1489.

[43] E. Laviron, A Multilayer Model for the Study of Space Distributed Redox Modified Electrodes. Part I. Description and Discussion of the Model, J. Electroanal. Chem. 112 (1980) 11–23. https://doi.org/10.1016/S0022-0728(80)80002-7.

[44] M. Tagliazucchi, E.J. Calvo, Charge transport in redox polyelectrolyte multilayer films: The dramatic effects of outmost layer and solution ionic strength, ChemPhysChem. 11 (2010) 2957–2968. https://doi.org/10.1002/cphc.201000172.

[45] M.N. Khan, S. Bhutto, Kinetic study of the oxidative decolorization of xylenol orange by hydrogen peroxide in micellar medium, J. Chil. Chem. Soc. 55 (2010) 170–175. https://doi.org/10.4067/s0717-97072010000200005.

[46] M. Lehene, D. Plesa, S. Ionescu-Zinca, S.D. Iancu, N. Leopold, S. V. Makarov, A.M.V.

Brânzanic, R. Silaghi-Dumitrescu, Adduct of Aquacobalamin with Hydrogen Peroxide, Inorg. Chem. 60 (2021) 12681–12684. https://doi.org/10.1021/acs.inorgchem.1c01483.

[47] A.W. Nichols, E.N. Cook, Y.J. Gan, P.R. Miedaner, J.M. Dressel, D.A. Dickie, H.S. Shafaat, C.W. Machan, Pendent Relay Enhances H_2O_2 Selectivity during Dioxygen Reduction Mediated by Bipyridine-Based Co-N_2O_2Complexes, J. Am. Chem. Soc. 143 (2021) 13065–13073. https://doi.org/10.1021/jacs.1c03381.

Graphical Abstract

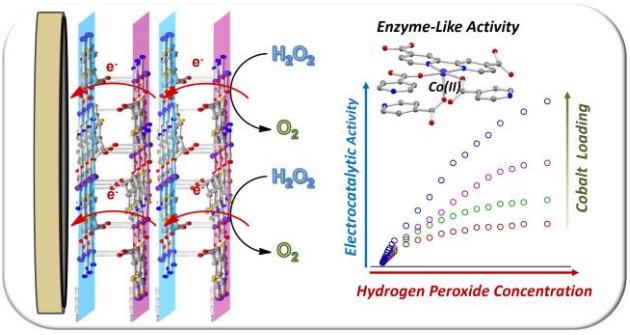

Supporting Information

Enzyme like Activity of Cobalt-MOF Nanosheets for Hydrogen Peroxide Electrochemical Sensing

Arismendy Portorreal-Bottier,[a] Silvia Gutiérrez-Tarriño,[b] Juan José Calvente,[a] Rafael Andreu,[a] Emilio Roldán,[a] Pascual Oña-Burgos,[b,c,*] José Luis Olloqui-Sariego[a,*].

[a]*Departamento de Química Física. Universidad de Sevilla. Profesor García González 1. 41012 Sevilla. Spain.*

[b]*Instituto de Tecnología Química, Universitat Politècnica de València-Consejo Superior de Investigaciones Científicas (UPV-CSIC), Avda. de los Naranjos s/n, 46022 Valencia, Spain.*

[c]*Departamento de Química y Física, Centro de Investigación CIAIMBITAL, Universidad de Almería, Ctra. Sacramento, s/n, 04120 Almería, Spain.*

1. Representation of the Double-Nanosheet Layer of the Cobalt MOF

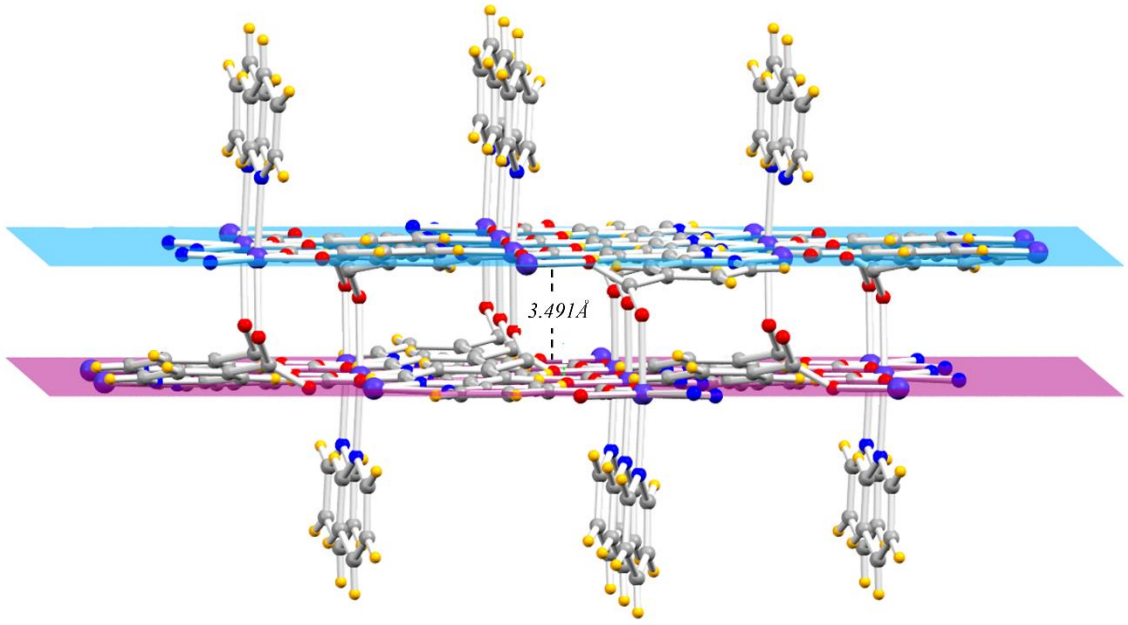

Figure S1. Representation of the calculated plane for each layer of the Co-MOF and measured distance between the 2 layer core.

2. Effect of water treatment on the Raman spectrum of the cobalt MOF

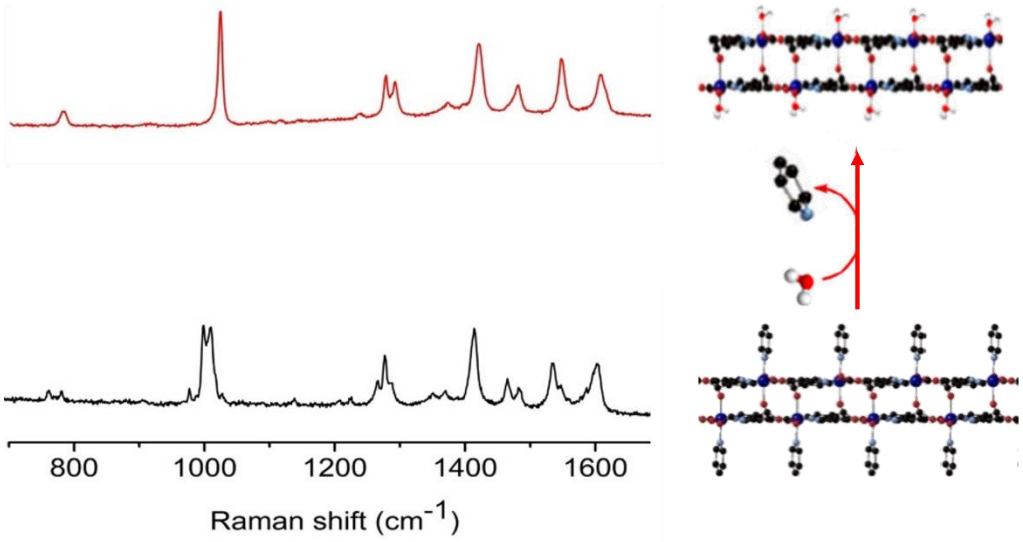

Figure S2. Raman spectra of the Co-MOF before (black) and after treatment with H_2O for 5 minutes giving rise to 2D-Co-MOF (red).

In the presence of water (red spectrum), the loss of the Raman bands associated with the axially coordinated pyridine ligands (768, 1010 and 1283 cm^{-1}) is evidenced, and the insensitivity of the bands associated with the bipyridine (774, 1022 and 1278 cm^{-1}) and carboxylic groups (1289, 1426, 1546 and 1615 cm^{-1}) indicates that the cobalt centers preserve their coordination to the bda and carboxylic ligands after treatment with water.

3. The effect of the potential scan rate on the voltammteric response of the 2D-Co-MOF@Nafion/PG electrode

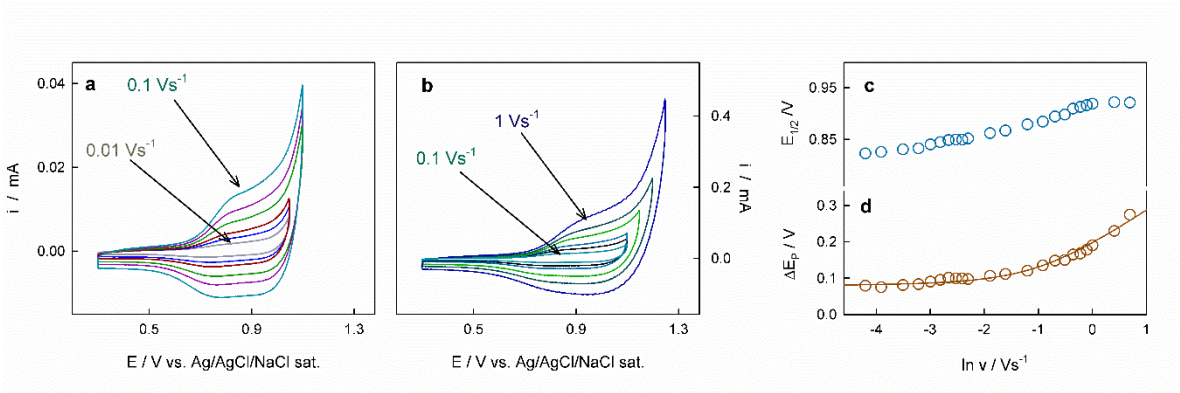

Figure S3. (a) and **(b)** Cyclic voltammograms of a pyrolytic graphite electrode modified with 2D-Co-MOF@Nafion recorded at various potential scan rates in an aqueous solution containing 0.1 M sodium phosphate buffer pH 7 at 25 ºC. **(c)** Midpoint potentials and **(d)** peak potential separation as a function of the potential scan rate. Solid line in Figure S3(d) is the theoretical fit computed from the Butler Volmer formalism with a k_s^{ap} value of ~1.5 s^{-1}.

4. Electrochemical Impedance Spectroscopy of the 2D-Co-MOF@Nafion/PG electrode

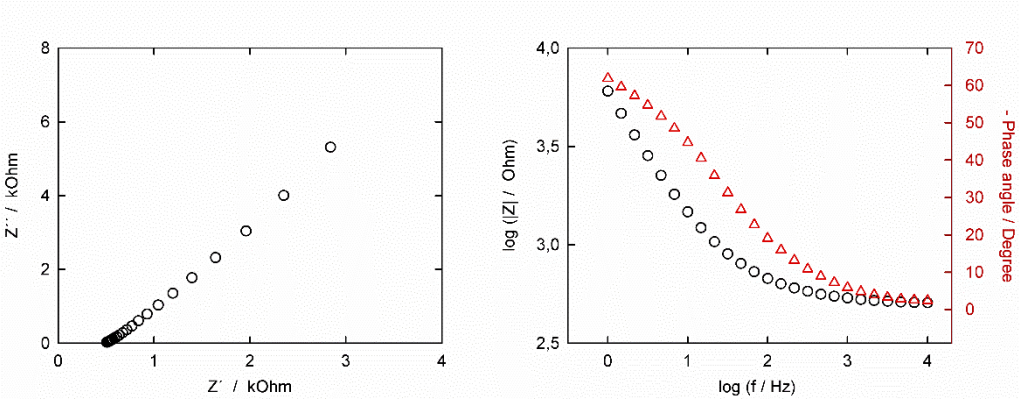

Figure S4. Nyquist and Bode plots recorded at 0.92V with a pyrolytic graphite electrode modified with the 2D-Co-MOF@Nafion composite in a solution containing 0.1 M SPB at pH 7 and 25 ºC.

The figure below shows the corresponding Nyquist and Bode plots. At the high-frequency limit, the Nyquist plot is characterized by a low Z' value, which reveals an efficient ionic migration rate across the MOF, and by a negligible depressed semicircle, which reveals a low charge-transfer resistance. Moreover, at the low-frequency range, the plot is characterized by a straight line with a slope of ~ 3.5, which is typical of a finite diffusion-controlled electron transfer. On the other hand, in the low frequency range, the Bode plot is characterized by a phase angle greater than 45 ºC and a linear decrease of |Z| with the frequency; whereas in the high frequency range, the phase angle approaches to zero and |Z| is slightly affected by the frequency; both features being indicative of a resistive behavior. Overall, these are the expected responses for the redox conversion of a 3D film controlled by the electron diffusion across the film, under conditions where both the ionic migration and the electron exchange between the electrode and the nearby redox centers are fast.

5. Quantification of the electrocatalytic current from the voltammetric response of the 2D-Co-MOF@Nafion/PG electrode

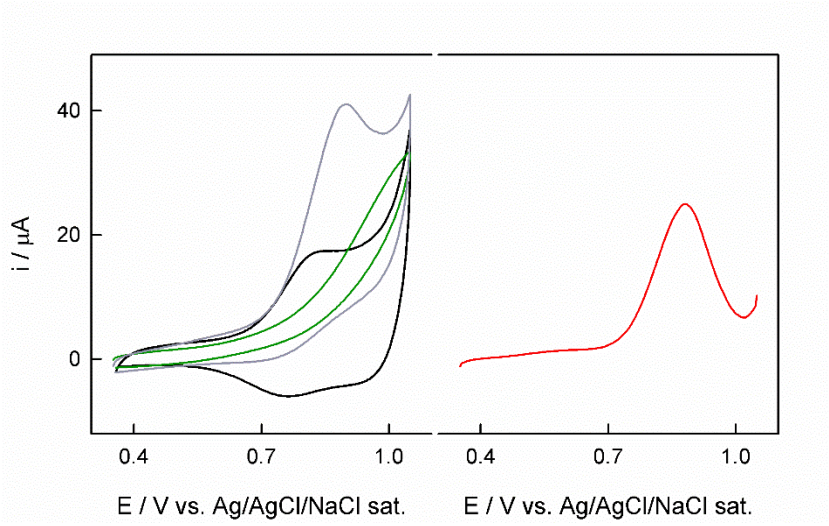

Figure S5. Illustration of the procedure used to quantify the electrocatalytic response of the 2D-Co-MOF@Nafion composite. (Left panel) Cyclic voltammograms recorded at 0.01 V s^{-1} of a pyrolytic graphite electrode coated with 2D-Co-MOF@Nafion composite in the absence (black line) or in the presence of a 4 mM hydrogen peroxide solution (grey line). Green line is the corresponding cyclic voltammogram of a pyrolytic graphite electrode coated only with Nafion recorded in the 4 mM hydrogen peroxide solution. (Right panel) The corresponding voltammogram obtained by subtracting the voltammograms recorded in the 4 mM hydrogen peroxide solution with the 2D-Co-MOF@Nafion-modified electrode and the electrode modified only with Nafion (for clarity, only anodic scan is shown).

6. Electrochemical Scanning Stability of the 2D-Co-MOF@Nafion/PG electrode

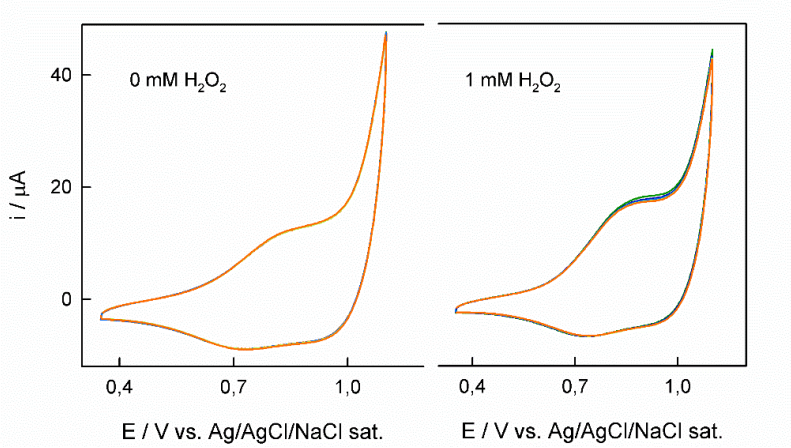

Figure S6. Five consecutives cyclic voltammograms recorded at 0.01 V s^{-1} of a pyrolytic graphite electrode coated with 2D-Co-MOF@Nafion composite in the presence of 0 mM (left panel) or 1mM (right panel) hydrogen peroxide concentration.Other experimental conditions, 0.1 M SPB pH 7.0 and 25 ºC.

7. Quantification of the Michaelis-Menten catalytic parameters for the electrocatalytic oxidation of hydrogen peroxide

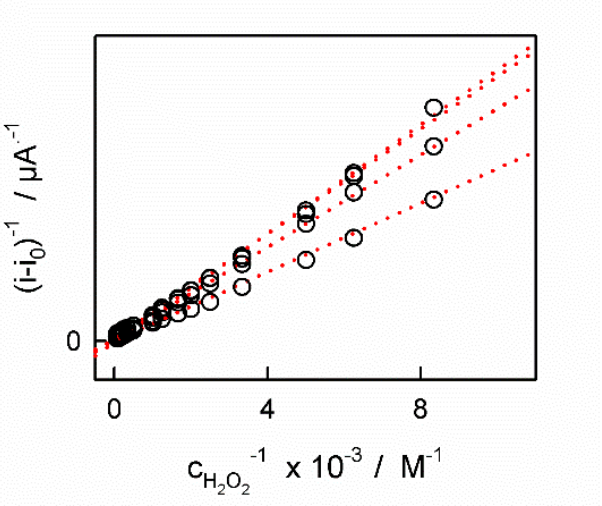

Figure S7. Double-reciprocal plots of the normalized catalytic current vs. hydrogen peroxide concentration depicted from the data of Figure 3b.

Table S1. Effect of Cobalt loading on the Michaelis-Menten catalytic parameters for the electrocatalytic oxidation of hydrogen peroxide

Cobalt loading /nmol	i_{max}/µA	K_M/mM
0.58	67	4
0.73	125	6
0.94	270	13
1.20	400	13

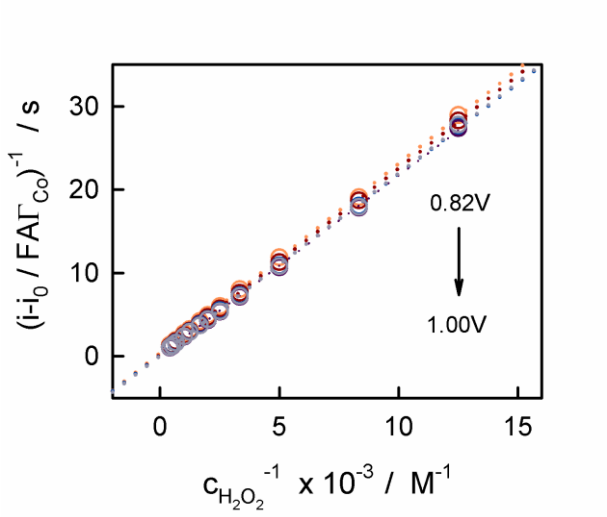

Figure S8. (a) Double-reciprocal plots of the normalized catalytic current vs. hydrogen peroxide concentration depicted from the data Figure 6.

Table S2. Effect of applied potential on the Michaelis-Menten catalytic parameters for the electrocatalytic oxidation of hydrogen peroxide.

Applied Potential /V	$(i_{max}/FA\Gamma_{Co})$ / s^{-1}	K_M/mM
0.82	1.3	2.8
0.84	2.2	4.8
0.86	3.1	7.0
0.88	3.6	7.8
0.90	4.2	9.1
0.92	4.5	9.7
0.94	4.7	10.0
0.96	4.9	10.3
0.98	5.1	10.7
1.00	5.1	10.7

8. Characterization of 2D-Co-MOF@Nafion composite after successive addition of hydrogen peroxide

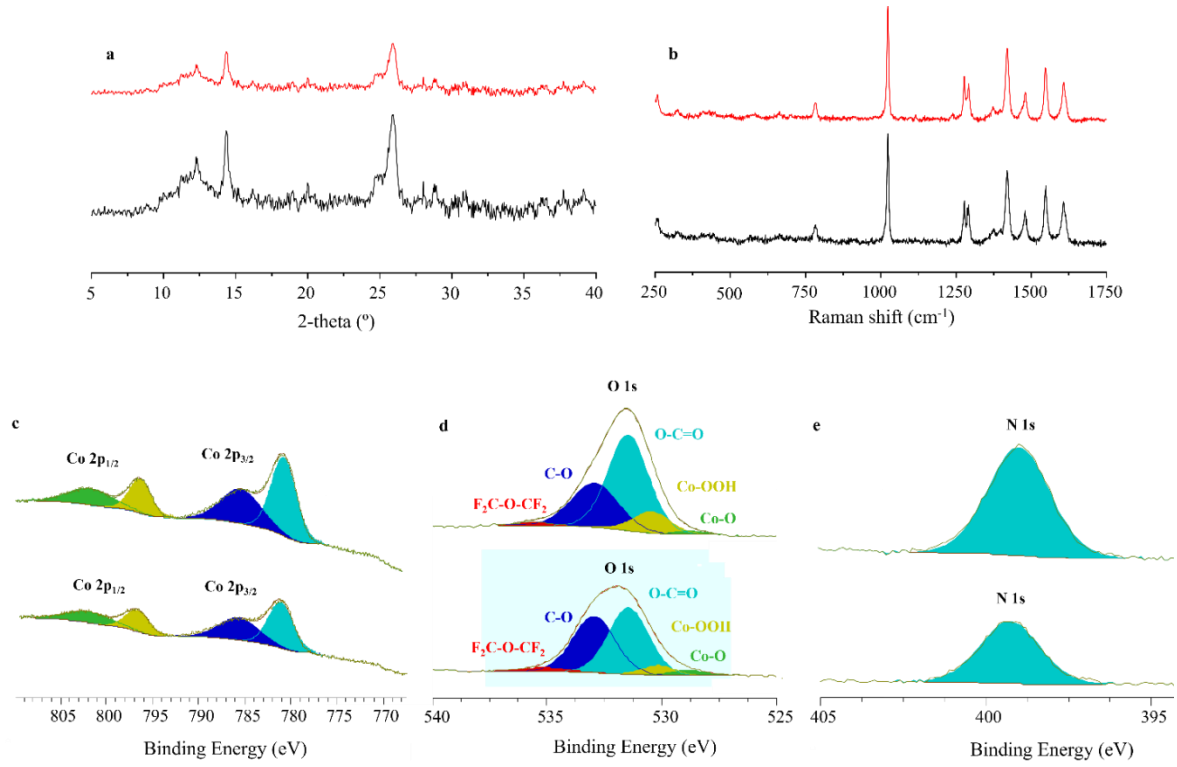

Figure S9. Characterization of 2D-Co-MOF@Nafion composite before (top) and after successive addition of hydrogen peroxide (bottom) by powder X-ray diffraction **(a)**, Raman spectroscopy **(b)** and X-ray photoelectron spectroscopy of Co 2p line **(c)**, O 1s line **(d)** and N 1s line **(e)**.

Table S3. Comparison of the operational parameters of Co-MOF-based electrochemical sensors for hydrogen peroxide detection.

Electrode	Solution	Reaction	Linear Range (mM)	Sensitivity (μA cm^{-2} mM)	LOD (μM)	Ref.
2D-CoMOF	0.1 M SPB, pH = 7.0	oxidation	0.005-1 1-12	570 395	38.1	This work
Co/DOBDC	0.1 M SPB, pH = 7.2	reduction	0.001–0.8	-	0.5	[1]
Co-NP@MOF-808	0.05 M SPB, pH = 7.3	oxidation	0.01-0.45	382.27	1.3	[2]
MOF Derived						
NCST-1	0.1 M NaOH	reduction	0.005–18	52.55	6.86	[3]
Co-MOF	0.1 M NaOH	reduction	0.005–9	83.10	3.76	[4]
Co-MOF	0.1 M KOH	oxidation	0.0005–0.832	551	0.69	[5]

9. Amperometric Hydrogen Peroxide Detection in Real Samples

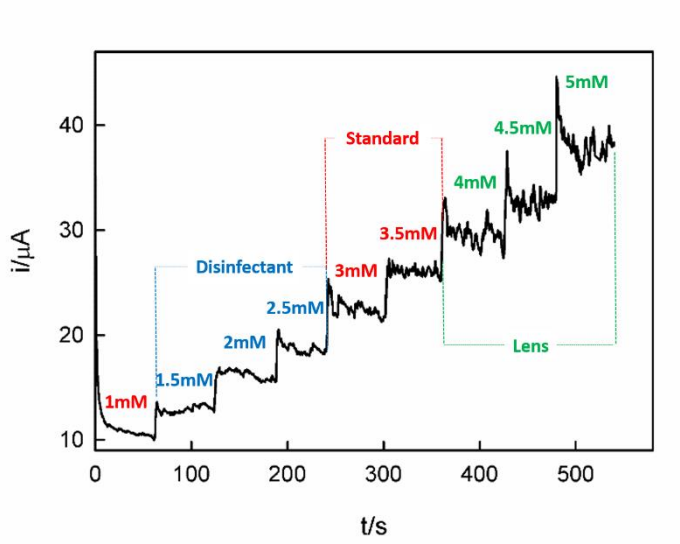

Figure S10. Chronoamperometric curve for the Co-MOF@Nafion-modified pyrolytic graphite electrode recorded at 0.90 V and 750 rpm after successive additions of the indicated samples (with 0.1M H_2O_2) to the initial cell solution containing 1 mM H_2O_2, 0.1 M SPB at pH 7, so that each addition corresponds to an increase of the H_2O_2 concentration in the cell of 500 µM.

Table S4. Comparison of the operational parameters of Co-MOF-based electrochemical sensors for hydrogen peroxide detection in real samples.

Solution	Added (µM)	Found (µM)	Recovery (%)	RSD (%)[a]
Disinfectant	500	484	97	3.2
Lens Cleaning	500	516	103	6.1

[a]Relative standard deviation estimated from three separated samples.

REFERENCES

[1] D. Zhang, J. Zhang, H. Shi, X. Guo, Y. Guo, R. Zhang, B. Yuan, Redox-active microsized metal-organic framework for efficient nonenzymatic H2O2 sensing, Sensors Actuators, B Chem. 221 (2015) 224–229. https://doi.org/10.1016/j.snb.2015.06.079.

[2] Y.S. Chang, J.H. Li, Y.C. Chen, W.H. Ho, Y. Da Song, C.W. Kung, Electrodeposition of pore-confined cobalt in metal–organic framework thin films toward electrochemical H2O2 detection, Electrochim. Acta. 347 (2020) 136276. https://doi.org/10.1016/j.electacta.2020.136276.

[3] Q.Q. Xiao, D. Liu, Y.L. Wei, G.H. Cui, A new multifunctional two-dimensional cobalt(II) metal–organic framework for electrochemical detection of hydrogen peroxide, luminescent sensing of metal ions, and photocatalysis, Polyhedron. 158 (2019) 342–351. https://doi.org/10.1016/j.poly.2018.11.016.

[4] L. Yang, C. Xu, W. Ye, W. Liu, An electrochemical sensor for H2O2 based on a new Co-metal-organic framework modified electrode, Sensors Actuators, B Chem. 215 (2015) 489–496. https://doi.org/10.1016/j.snb.2015.03.104.

[5] B. Liu, X. Wang, Y. Zhai, Z. Zhang, H. Liu, L. Li, H. Wen, Facile preparation of well conductive 2D MOF for nonenzymatic detection of hydrogen peroxide: Relationship between electrocatalysis and metal center, J. Electroanal. Chem. 858 (2020) 113804. https://doi.org/10.1016/j.jelechem.2019.113804.